International Journal of Mass Spectrometry 443 (2019) 22–31

Contents lists available at ScienceDirect

International Journal of Mass Spectrometry

journal homepage: www.elsevier.com/locate/ijms

UV-vis action spectroscopy and structures of hydrogen-rich 2′-deoxycytidine dinucleotide cation radicals. A difficult case

Yang Liu, Joseph A. Korn, František Tureček*

Department of Chemistry, Bagley Hall, Box 351700, University of Washington, Seattle, WA, 98195-1700, USA

ARTICLE INFO

Article history:
Received 14 April 2019
Received in revised form
20 May 2019
Accepted 29 May 2019
Available online 30 May 2019

Keywords:
Dinucleotide cation radicals
UV-Vis action spectroscopy
Electron transfer dissociation
Born-oppenheimer molecular dynamics
Time-dependent density functional theory

ABSTRACT

Hydrogen-rich cation radicals of 2′-deoxycytidine dinucleotide, $(dCC + 2H)^{+\bullet}$, were generated by electron transfer dissociation of their doubly charged complexes with crown ethers and found to be stable in the gas phase. The $(dCC + 2H)^{+\bullet}$ ions were calculated to be formed with ca. 280 kJ mol^{-1} internal energy that was rapidly dissipated below a 130 kJ mol^{-1} energy threshold for the lowest-energy dissociation by loss of water. UV-vis action spectroscopy was applied to monitor several photodissociation channels of $(dCC + 2H)^{+\bullet}$ and to compose spectra that showed distinct absorption bands at 220, 270, 290, and 350 nm, and a broad featureless band at 500-700 nm. UV-vis action spectra were also obtained for the $(dCC - H_2O + 2H)^{+\bullet}$ cation radical that showed bands at 225, 270, 330, 430, and 530 nm. Born-Oppenheimer molecular dynamics and density functional theory (DFT) calculations were employed to generate a complete set of tautomeric $(dCC + crown + 2H)^{2+}$ precursor dications and identify the lowest-energy structures in the gas phase and aqueous solution that were the cytosine N-3-H tautomers. Calculations also indicated that cytosine cations and radicals in the lowest-energy $(dCC + 2H)^{+\bullet}$ ions were N-3-H tautomers. Absorption spectra of several $(dCC + 2H)^{+\bullet}$ tautomers were obtained by time-dependent DFT calculations that provided a limited match with the action spectrum. In contrast, a satisfactory match was obtained for the action and absorption spectra of $(dCC - H_2O + 2H)^{+\bullet}$ fragment ions. $(dCC + 2H)^{+\bullet}$ represents a difficult case because of a multitude of cation and radical tautomers to be analyzed and the propensity for consecutive photofragment dissociation upon photon absorption.

1. Introduction

Capture of low-energy secondary electrons is one of the principal mechanisms of DNA damage [1]. When studied in frozen glasses, electron capture by nucleotides was found to result in nucleobase loss from the transient anion radicals [2], forming 1′-deoxyribose radicals that could undergo further reactions. When formed in a protic medium, the basic nucleobase anion radicals can undergo rapid protonation, forming radical hydrogen atom adducts [3]. DNA-electron interactions have been extensively studied by pulse radiolysis that produced complex mixtures and most studies relied on electron paramagnetic resonance spectroscopy to characterize the radical species [4-6]. Hydrogen-rich nucleobase radicals have also been generated by femtosecond electron transfer to mass-selected nucleobase cations and characterized by neutralization-reionization mass spectrometry [7-10] and ab initio theoretical calculations [11]. Hydrogen-rich DNA cation radicals represent a novel type of transient intermediates in which one nucleotide carries a charge in the form of a protonated nucleobase while another nucleotide has been converted to a hydrogen atom adduct. By having both the charged and radical moieties, hydrogen-rich DNA cation radicals, denoted as $(dXX + 2H)^{+\bullet}$, X = nucleobase, are particularly suited for mass spectrometric studies. Recently, we have reported that hydrogen-rich cation radicals can be efficiently generated by electron transfer dissociation of doubly charged DNA dinucleotides with crown ethers. Cation radicals of $(dAA + 2H)^{+\bullet}$, chimeric RNA dinucleotides [12], $(dGG + 2H)^{+\bullet}$, $(dGC + 2H)^{+\bullet}$, and $(dGC + 2H)^{+\bullet}$ [13] have been generated and characterized by UV-vis photodissociation action spectroscopy [14-16].

The cytosine rings in dideoxycytidine ions and radicals present a particular challenge for the generation of dications and their reduction by electron transfer. Neutral cytosine is known to exist as N-1-H, O-2-H, N-3-H, and N-4-imine tautomers of very similar relative energies in the gas phase, as elucidated by VUV synchrotron ionization [17,18], microwave spectroscopy [19], and ab initio

* Corresponding author.
E-mail address: turecek@chem.washington.edu (F. Tureček).

https://doi.org/10.1016/j.ijms.2019.05.016
1387-3806/

calculations [20-24]. Cytosine cation radicals that were generated by intramolecular electron transfer in gas-phase Cu complexes have been shown by infrared multiphoton dissociation (IRMPD) and single-photon UV-Vis action spectroscopies to consist of a mixture of tautomers [25]. Ab initio calculations of cytosine cation radicals pointed to N-3-H and O-2-H tautomers as the lowest-energy structures [26]. Cytosine protonation by electrospray ionization has been shown by IRMPD spectroscopy to produce gas phase ions as a mixture of O-2-H and N-3-H tautomers [27,28]. Hydrated cytosine ions [29,30], cytidine nucleosides [31] and nucleotides [32] have all been shown by IRMPD spectroscopy to consists of N-3-H and O-2-H protonated forms in the gas phase. Hydrogen-rich cytosine and 1-methylcytosine radicals have been generated in the gas phase by femtosecond electron transfer and characterized by tandem mass spectra after reionization [33,34]. Ab initio [35] and density functional theory [36] calculations of cytosine radicals have identified the N-1-H, N-3-H tautomer as the lowest-energy structure whereas hydrogen atom adducts to C-5, C-6, and several other tautomeric combinations were >30 kJ mol^{-1} higher in energy. Photoexcitation of cytosine has attracted substantial interest, and the studies have revealed that the excited electronic states underwent fast decay with rates and branching ratios that depended on the tautomer structure [37-44]. The previous data indicated that the formation of cytosine ions, cation radicals, and their electronic structure and behavior may be complicated, in particular if the cytosine rings are incorporated in di- or larger oligonucleotides. Here we report an experimental and computational study addressing the complexities of the formation, action spectra, and comprehensive structure and energy analysis of hydrogen-rich 2′-deoxycytidine dinucleotide ions and radicals.

2. Experimental

2.1. Materials and methods

2′-deoxycytidine dinucleotide (dCC) was custom made by Integrated DNA Technologies (Coralville, IA) and used as received. 18-Crown-6-ether (CE) and 2,3:11,12-dibenzo-18-crown-6-ether (DBCE) were purchased from Sigma-Aldrich (Milwaukee, WI) and used as received. The dinucleotide and crown ethers in an approximately 1:1.2 molar ratio were dissolved in 80:20:1 mixture of acetonitrile:water:acetic acid to achieve concentrations in the 20-50 μM range. The solutions were electrosprayed into the ion trap mass spectrometer. Electron transfer dissociation (ETD) and photodissociation mass spectra were measured on two different instruments. One was a modified ThermoElectron Fisher (San Jose, CA, USA) LTQ-XL ETD linear ion trap mass spectrometer that was furnished with an external EKSPLA NL301G (Altos Photonics, Bozeman, MT) Nd-YAG laser source operating at a frequency of 20 Hz with a 3–6 ns pulse width, and an optical parametric oscillator system, as described previously [14]. The other instrument was a Bruker amaZon Speed 3D ion trap mass spectrometer that was equipped with windows allowing laser beam entrance to the ion trap and furnished with the same EKSPLA NL301G laser. The operating procedures for obtaining UV-vis action spectra in the 210-700 nm region on both instruments have been described [45,46]. The electrospray ion source, and ion transfer ion optical elements were tuned to optimize the formation of doubly charged complexes. Doubly charged ions were isolated by mass in the ion trap and allowed to react with fluoranthene anions for 100-200 ms. The charge-reduced cation radicals formed were isolated by mass and exposed to laser pulses for photodissociation. The number of laser pulses used for photodissociation varied from 1 pulse in the 400-700 nm region, 1-5 pulses in the 210-350 nm region, to 5 pulses in the 353-400 region. Each wavelength point in the UVPD spectrum consisted of >100 accumulated and averaged scans. The reported action spectra are averages of two reproduced measurements obtained on different days.

2.2. Calculations

Born-Oppenheimer molecular dynamics of doubly protonated (dCC + crown ether) complexes was run with semiempirical quantum PM6 calculations [47] that were augmented by including dispersion and hydrogen bonding interactions, D3H4 [48]. BOMD trajectories were run at 1 fs steps for 20 ps with energy conservation by weak coupling to a Berendsen thermostat [49], generating 20000 conformer snapshots for each tautomeric ion. These calculations were run with MOPAC [50] that was coupled to the Cuby4 platform [51]. Two hundred snapshots were selected from each trajectory, the structures were fully gradient-optimized with PM6-D3H4 and sorted out by their secondary and supersecondary structural similarities. Several low-energy complex structures were selected for each tautomer and their geometries were optimized with B3LYP [52] and the 6-31G (d,p) basis set to yield harmonic frequencies. The complex structures were further reoptimized with ωB97X-D [53] and M06-2X [54], both with the 6-31 + G (d,p) basis set, to evaluate electronic energies including dispersion interactions. Further sets of energies were obtained by single-point M06-2X/6-311++G (2d,p) and MP2(frozencore)/6-311++G (2d,p) calculations [55]. Contamination by higher spin states in the UMP2 calculations was treated by standard spin annihilation methods (PMP2 [56,57]) and further checked by restricted open-shell MP2 (ROMP2) single-point calculations [58]. The electronic, vibrational, and rotational energies and entropies were combined to yield relative free energies at the experimental temperature of 310 K. To assess solvent effects, we performed single-point energy self-consistent reaction field calculations using the polarizable continuum model [59] with van der Waals surfaces, water as the dielectric, and structures optimized in the gas-phase and dielectric. Vertical excitation energies and oscillator strength were calculated by time-dependent density functional theory (TD-DFT [60]) using M06-2X/6-31 + G (d,p). Our previous investigations of electronic excitations in nucleobase, nucleoside, and dinucleotide radicals have indicated that TD-DFT M06-2X/6-31 + G (d,p) calculations provide reliable excitation parameters when benchmarked against higher-level, equation-of-motion coupled-cluster (CCSD), calculations [61]. All the thermochemical calculations were performed using the Gaussian 16 (Revision A.03) suite of programs [62].

3. Results and discussion

3.1. Ion formation

Electrospray ionization of dCC-crown ether mixture solutions yielded doubly charged complexes that were isolated by mass and subjected to ion-ion reactions with fluoranthene anions. ETD [63] resulted in charge reduction and elimination of the crown ligand, as shown for the complex with dibenzocrown ether (DBCE), $(dCC + 2H + DBCE)^{2+}$ at *m/z* 439 (Fig. 1a). The complex with 18-crown-6-ether (CE) gave similar results. In both cases ETD generated the $(dCC + 2H)^{+\bullet}$ cation radical at *m/z* 518 as a major product in an excellent yield. In contrast, ETD of $(dCC + 2H)^{2+}$ resulted in complete dissociation (Figure S1, Supplementary Information). The other products from ETD of the crown ether complex were $(dCC + H)^{+}$ (*m/z* 517) and $(dCC + H + crown)^{+}$ at *m/z* 877 and 781 for DBCE and CE, respectively. The $(dCC + 2H)^{+\bullet}$ cation radical was isolated by mass and probed by collision-induced dissociation, CID-MS^3 (Fig. 1b). This produced a dominant fragment ion by loss of water (*m/z* 500), and further fragment ions by loss of $(C + H)^{\bullet}$

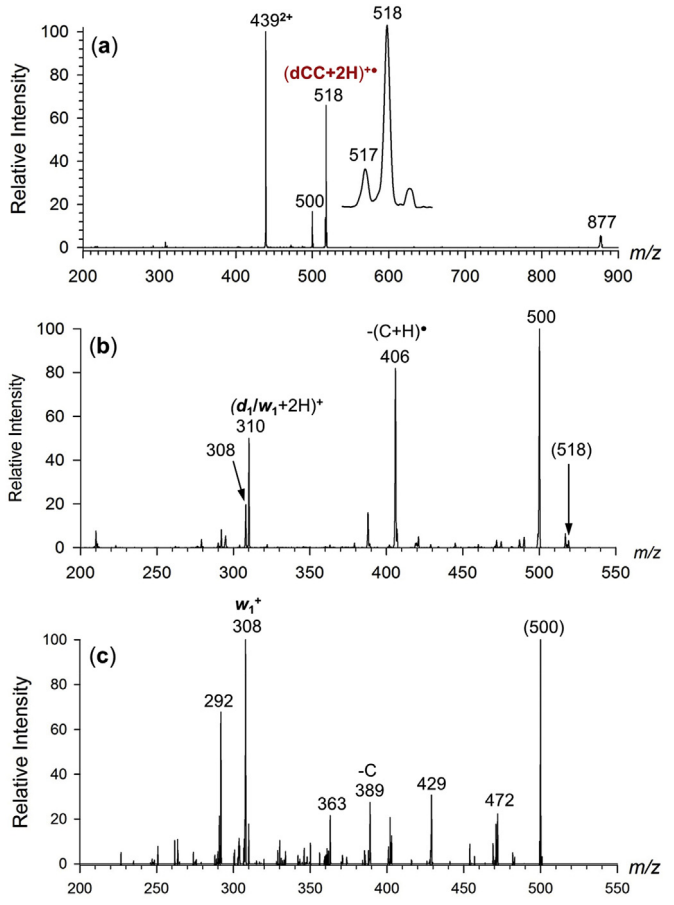

Fig. 1. (a) ETD spectrum (fluoranthene, 150 ms) of $(dCC + DBCE + 2H)^{2+}$ complex at *m/z* 439. (b) CID-MS^3 spectrum of $(dCC + 2H)^{+\bullet}$ ion at *m/z* 518. (c) CID-MS^4 spectrum of the $(dCC - H_2O + 2H)^{+\bullet}$ ion at *m/z* 500.

radicals (*m/z* 406), and their secondary products by loss of water (*m/z* 388). Backbone dissociations formed the $(d_1/w_1 + 2H)^+$ (*m/z* 310), $(d_1/w_1)^+$ (*m/z* 308), and a_1/z_1 (*m/z* 210) ions. The backbone ions assignment followed the standard nomenclature [64,65]. Interestingly, most of the backbone fragment ions were even-electron species, indicating loss of neutral radicals from $(dCC + 2H)^{+\bullet}$.

The prominent $(dCC + 2H - H_2O)^{+\bullet}$ cation-radicals were further investigated by CID-MS^4 that yielded the mass spectrum shown in Fig. 1c. This displayed a dominant ion at *m/z* 308 that we assigned as d_1/w_1, and several other fragment ions formed by combined losses of CO, C_2H_3O, and cytosine. Interestingly, the $(d_1/w_1 + 2H)^+$ ion from $(dCC + 2H)^{+\bullet}$ appeared as $(d_1/w_1 - H_2O + 2H)^+$ at *m/z* 292 in the CID spectrum of $(dCC + 2H - H_2O)^{+\bullet}$ (Fig. 1c). These fragmentations involving double hydrogen transfer have not been observed in the CID spectra of closed-shell DNA cations [65] and appear to be associated with the radical cytosine rings in $(dCC + 2H)^{+\bullet}$ and $(dCC + 2H - H_2O)^{+\bullet}$. We will discuss the possible reaction sequence leading to these fragmentations later in the paper.

3.2. Photodisociation action spectra

Photodissociation of mass-selected $(dCC + 2H)^{+\bullet}$ ions was investigated in the wavelength range of 210-700 nm, covering the valence-electron excitations in the cation-radicals. The major photodissociation products were observed at *m/z* 500, 406, 310, 308, and 292 that were analogous to fragment ions produced by CID. The *m/z* 406 and 500 channels turned out to be problematic in following the absorption by $(dCC + 2H)^{+\bullet}$, as they showed unusual characteristics over most of the covered wavelength region. The dominant *m/z* 500 channel further displayed gradually increasing dissociation at $\lambda > 500$ nm which was unprecedented in the action spectra of other dinucleotide cation radicals [12,13]. The action spectrum that was combined from the *m/z* 292, 308, 310, 406 and 500 channels showed distinct bands at 350, 290, 270, and 220 nm (Fig. 2a), in addition to a broad featureless band at 500-700 nm. Light absorption at 350 and 270 nm was pronounced in the *m/z* 308 and 310 channels (Fig. 2b), whereas the 220-nm band was in part contributed by the *m/z* 292 channel (Fig. 2c).

The photodissociation characteristics of the fragment ion by loss of water (*m/z* 500) was further investigated by UVPD-MS^4. The action spectrum showed bands at 330, 270 and 225 nm that were analogous to those found for $(dCC + 2H)^{+\bullet}$. In addition, weak bands were observed at 530 and 430 nm (Fig. 3a). The main bands in the action spectra of $(dCC + 2H)^{+\bullet}$ and the *m/z* 500 fragment ion indicated similar chromophores that were associated with the pertinent radical moieties.

3.3. Dication structures

To characterize the absorption properties of $(dCC + 2H)^{+\bullet}$ we undertook an extensive computational analysis of the structures

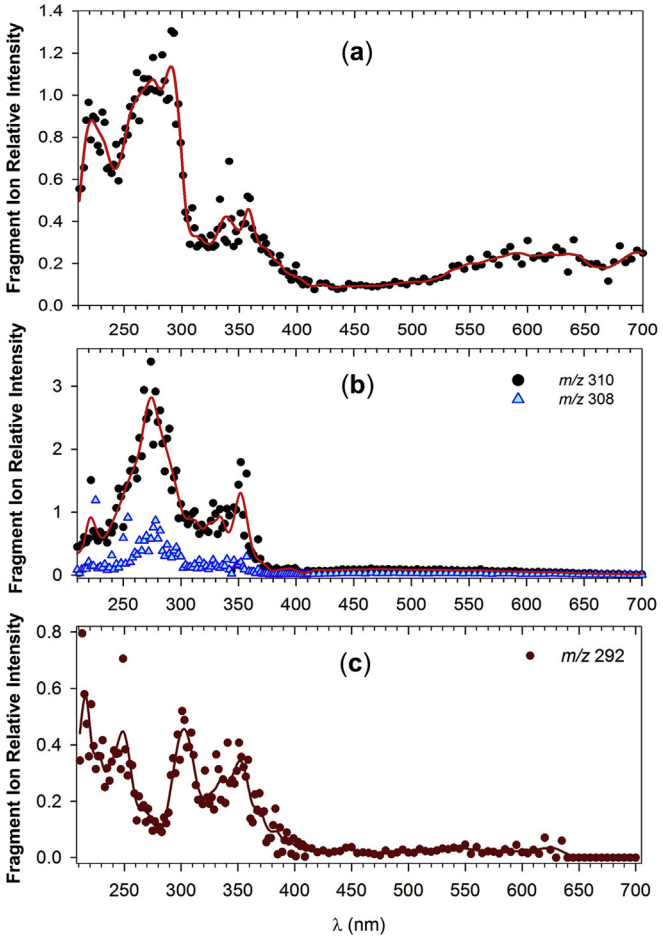

Fig. 2. UV-Vis action spectra of $(dCC + 2H)^{+\bullet}$. (a) Sum of photofragment ion intensities.; (b) Relative intensities of *m/z* 308 and 310 photofragment ions. (c) Relative intensities of *m/z* 292 photofragment ions.

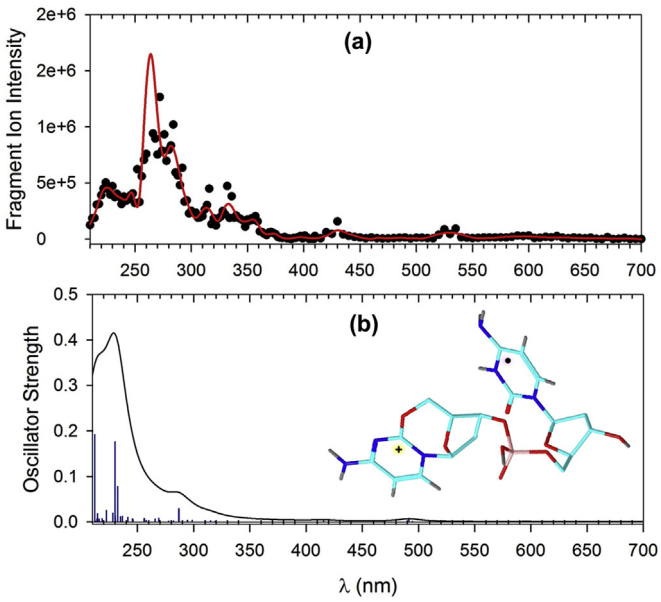

Fig. 3. (a) Action spectrum of the $(dCC - H_2O + 2H)^{+\bullet}$ from ETD-CID-MS^4. (b) TD-DFT . M06-2X/6-31 + G (d,p) absorption spectrum of **17**. The lines were artificially broadened by convolution with a Lorentzian function at 12 nm full-width at half maximum.

involved in the ion formation, photoexcitation, and dissociation. Our goal was to first establish the thermodynamically most stable isomers of the $(dCC + crown + 2H)^{2+}$ precursor ions to determine the protonation sites, cytosine tautomers and crown-ether attachment sites. This was followed by conformational analysis of energy-selected $(dCC + 2H)^{+\bullet}$ cation radicals and several products of their isomerization by proton and hydrogen atoms migration. In the last step, we performed TD-DFT calculations of 45 excited states of several representative $(dCC + 2H)^{+\bullet}$ isomers.

To begin with the $(dCC + 2H + crown)^{2+}$ precursor ions, we used BOMD to generate conformers of all 8 combinations of complexes consisting of 4 cytosine O-2 and N-3-protonated tautomers, each with a *3′*- or *5′*-crown ether ligand. As reported previously [13,14], dinucleotide dication complexes with 18-crown-6-ether and 2,3:11,12-dibenzo-18-crown-6-ether showed very similar energy rankings of tautomer and coordination isomers, and so we used the smaller 18-crown-6-ether as an economical surrogate in these extensive calculations. The DFT-calculated free energies of fully optimized gas-phase complexes revealed a distinct preference for structures in which the crown ether was coordinated to the N-3-H protonated cytosine in the *3'* (**1a,b**) or *5′* positions (**2a**,**b**) (Fig. 4, Table 1). This distinction was further amplified by solvent effects in water where structures **1a, 1b** represented the lowest free-energy isomers (Table 1). Complexation to the N-3-H cytosine cation at the *3′* and *5′* termini in tautomers having the other cytosine protonated at O-2-H also gave rise to low-energy gas-phase structures

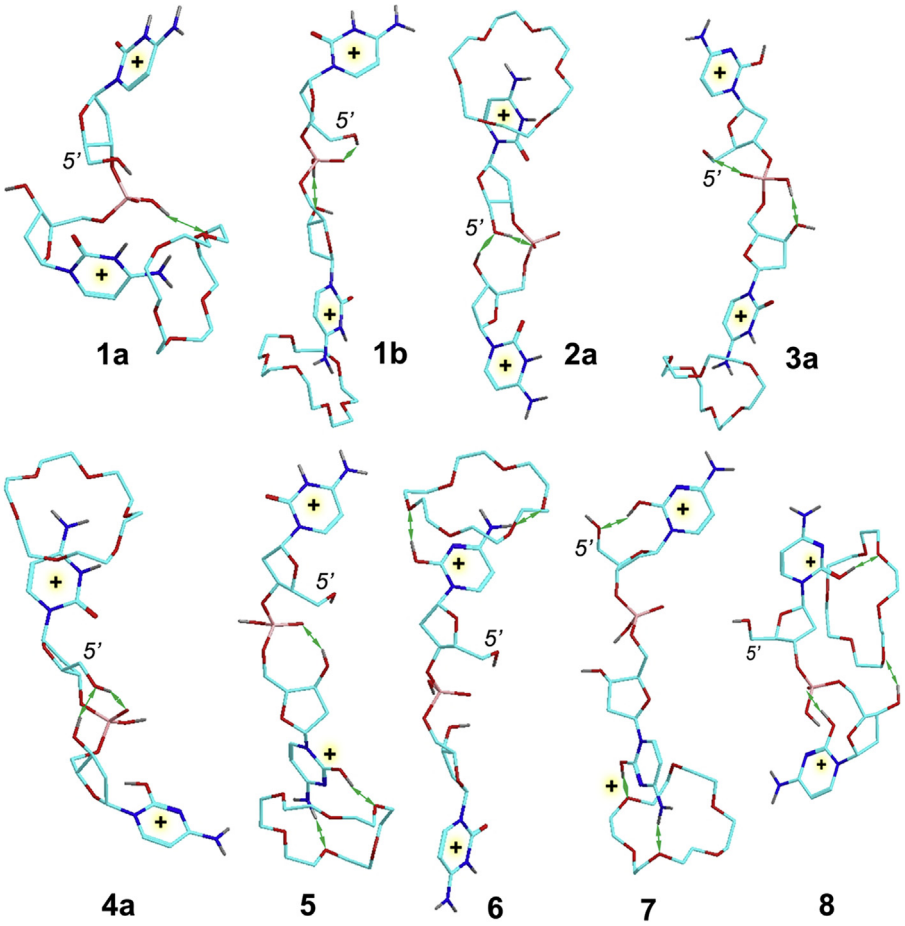

Fig. 4. ωB97X-D/6-31 + G (d,p) optimized structures of selected low-energy $(dCC + crown + 2H)^{2+}$ ions. Atom color coding is as follows: cyan = C, gray = H, blue = N, red = O, pink = P. Only exchangeable (N–H, O–H) hydrogens are shown. Major hydrogen bonds are indicated by green arrows. (For interpretation of the references to color in this figure legend, the reader is referred to the Web version of this article.)

Table 1
Relative energies of $(dCC + CE + 2H)^{2+}$ ions.[a]

Type	Conformer	Relative Energy[b,c]			
		Gas phase		Water	
		ΔH (0)[d]	ΔG (310)[e]	ΔG_{aq} (310)[f]	
N-3-H, N-3-H, 3′-crown	**1a**	0.3	–11	7.1[g]	8.5[h]
	1b	0	0	0	0
N-3-H, N-3-H, 5′-crown	**2a**	17	7.5	15	19
	2b	26	15	19	13
O-2-H, N-3-H, 3′-crown	**3a**	14	–3.2	42	43
	3b	10	–0.5	50	55
N-3-H, O-2-H, 5′-crown	**4a**	14	7.1	40	46
N-3-H, O-2-H, 3′-crown	**5**	67	58		
O-2-H, N-3-H, 5′-crown	**6**	72	60		
O-2-H, O-2-H, 3′-crown	**7**	99	89		
O-2-H, O-2-H, 5′-crown	**8**	74	73		

[a] CE stands for 18-crown-6-ether.
[b] Energies in kJ mol^{-1} for ωB97X-D/6-31 + G (d,p) optimized structures.
[c] Including B3LYP zero-point vibrational energies.
[d] Relative enthalpies in the gas phase at 0 K.
[e] Relative free energies in the gas phase at 310 K.
[f] Including solvation energies in the water dielectric.
[g] Optimized with inclusion of solvation by water via the polarizable continuum model.
[h] PCM single-point energies on gas-phase optimized structures.

(**3a, 3b** and **4a,** Fig. 4). The reason for the stability of the N-3-H coordinated complexes in the gas phase was evident from the hydrogen bonding to the crown ether, as the N-3-H protonated cytosine ring can develop three strong hydrogen bonds to the crown-ether oxygens, one by N-3-H and two by protons of the NH_2 group (Fig. 4). In contrast, coordination to the O-2 protonated cytosine ring in **5**-**8** was less favorable, as the cytosine ring developed only two hydrogen bonds to the crown ligand, one by the O-2-H and the other by one of the NH_2 protons (Fig. 4). The reason for the preferential coordination to the 3′-N-3-H protonated cytosine, e.g. **1a, 1b** versus **2a**, was less obvious and was likely due to a combination of several subtle effects. In summary, coordination by the crown ether in combination with solvent effects steered the cytosine protonation in dCC to the N-3 positions favoring a single type of the dinucleotide ion tautomer.

3.4. Cation radical formation and structures

Electron attachment to the $(dCC + 2H + crown)^{2+}$ ions was investigated for the lowest energy structure **1a**. According to ωB97X-D calculations, the reducing electron entered the non-coordinated cytosine ring (**1r**, Scheme 1). This was analogous to electron capture by other dicationic crown-ether complexes where solvation by the electron-donating crown ether was shown to stabilize the ion, decreasing its recombination energy, and steering the incoming electron into the non-solvated charged group [66]. Electron attachment to $(dCC + crown + 2H)^{2+}$ was associated with an adiabatic recombination energy that was calculated as $RE_{ad-iab} = 6.08$ eV. Considering the electron affinity of the fluoranthene electron donor, EA = 0.63 eV [67], the vibrational excitation energy in the $(dCC + crown + 2H)^{+\bullet}$ intermediate complex **1r** can be estimated [68] as $E_{exc} \approx (6.08 - 0.63) = 5.45$ eV (526 kJ mol^{-1}) which is added to the 310 K ro-vibrational enthalpy in **1a** (120 kJ mol^{-1}). The high vibrational energy of charge-reduced **1r** drove the dissociation of **1r**, overcoming the binding energy of the crown ether ($\Delta H_{dis,310} = 143$ kJ mol^{-1}, $\Delta G_{dis,\ 310} = 70$ kJ mol^{-1}, by ωB97X-D/6-31 + G (d,p) including counterpoise corrections), and resulting in ca. 503 kJ mol^{-1} non-fixed energy which was partitioned between $(dCC + 2H)^{+\bullet}$ and the crown ether. From the energy partition terms based on the number of vibrational degrees of freedom in $(dCC + 2H)^{+\bullet}$ and the crown ether, 180 and 144, respectively [69], we estimated the initial excitation energy in

Table 2
Relative energies of $(dCC + 2H)^{+\bullet}$ cation radicals.

Ion/Reaction	Radical Site	Relative Energy[a,b]			
		ωB97X-D	M06-2X	PMP2	ROMP2
9a	5′	0ω	0	0	0
9b	5′	19	16	17	18
9c	5′	59	25	21	22
9d	5′	36	39		
10	3′	31	29	28	27
11a	3′	54	35	34	33
11b	3′	53	48		
12	5′	63	49		
13	5,5-H_2	37	34	31	38
14	6,6-H_2	56	58		
15	5′	73	61		
16	3′	97	87		
TS (**9a** →**13**)		97	103	92	96
9a → **17** + H_2O		149	130	127	126
9a → **18** + H_2O		199	188	189	196
17 → *m/z* 389 + cytosine		146	130	154	161
17 → **19** + **20**		170	154	167	156
9a → **19** + **20**		318	284	294	282

[a] Energies in kJ mol^{-1}.
[b] Including B3LYP zero-point vibrational energies and referring to 0 K in the gas phase.

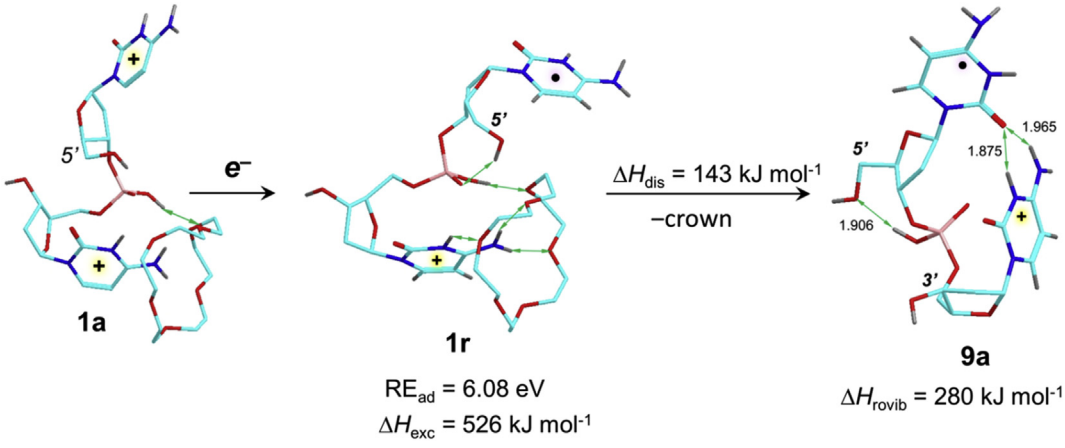

Scheme 1. Electron transfer and dissociation of the $(dCC + crown + 2H)^{2+}$ complex **1a**.

$(dCC + 2H)^{+\bullet}$ formed by ETD to be ca. 503 × 180/(180 + 144) ≅ 280 kJ mol^{-1}.

Under the conditions in the ion trap, the excitation can drive dissociations and isomerizations of the $(dCC + 2H)^{+\bullet}$ cation radical, or be dissipated by collisions with the bath gas [69,70].

Geometry optimization of $(dCC + 2H)^{+\bullet}$ cation radicals yielded several structures that differed in their conformation and position of the charging proton and odd electron. In general, one-electron reduction was expected to occur in one of the O-2 or N-3-protonated cytosine rings which was consistent with the calculated cation-radical structures. The relative energies quoted in the text refer to M06-2X/6-311++G (2d,p) calculations, energies from the other calculations are listed in Table 2. The calculations pointed to the 5′-N-3-H-cytosine radicals **9a** (Fig. 5) and **9b** (Figure S2) as the lowest-energy isomers (Table 2). Note that the unpaired electron distribution in **9a** and **9b** directly correlated with that in the charge-reduced crown complex **1r** (Scheme 1). The position of the radical was evident from the puckered conformation of the charge-reduced ring and confirmed by the calculated atomic spin densities that showed >98% of the unpaired spin to be located in the 5′-cytosine ring. The 3′-N-3-H-cytosine radicals were ca. 30 kJ mol^{-1} higher in energy for the most stable conformer (**10**, Fig. 5). Isomeric cation-radicals with an O-2-protonated ring in the 3'- (**12**) or 5′-position (**11a**) had the radical in the complementary N-3-H ring, but were overall >35 kJ mol^{-1} less stable than **9a**. The ordering of relative energies for the cytosine radical tautomers in $(dCC + 2H)^{+\bullet}$ followed that of cytosine radicals where the N-1-H, N-3-H tautomer is the most stable structure [33,36]. It is noteworthy that all the low-energy $(dCC + 2H)^{+\bullet}$ structures comprised hydrogen bonds between the charged ring as a proton donor and the reduced ring as a proton acceptor. The dramatic structure change from the mostly extended dications to folded cation radicals can be attributed to the combined effects of canceling the Coulomb repulsion between the charged cytosine rings upon reduction, and allowing hydrogen bonding between the charged and radical moieties, as in structures **9**-**11**, **15**, and **16** (Fig. 5). This was

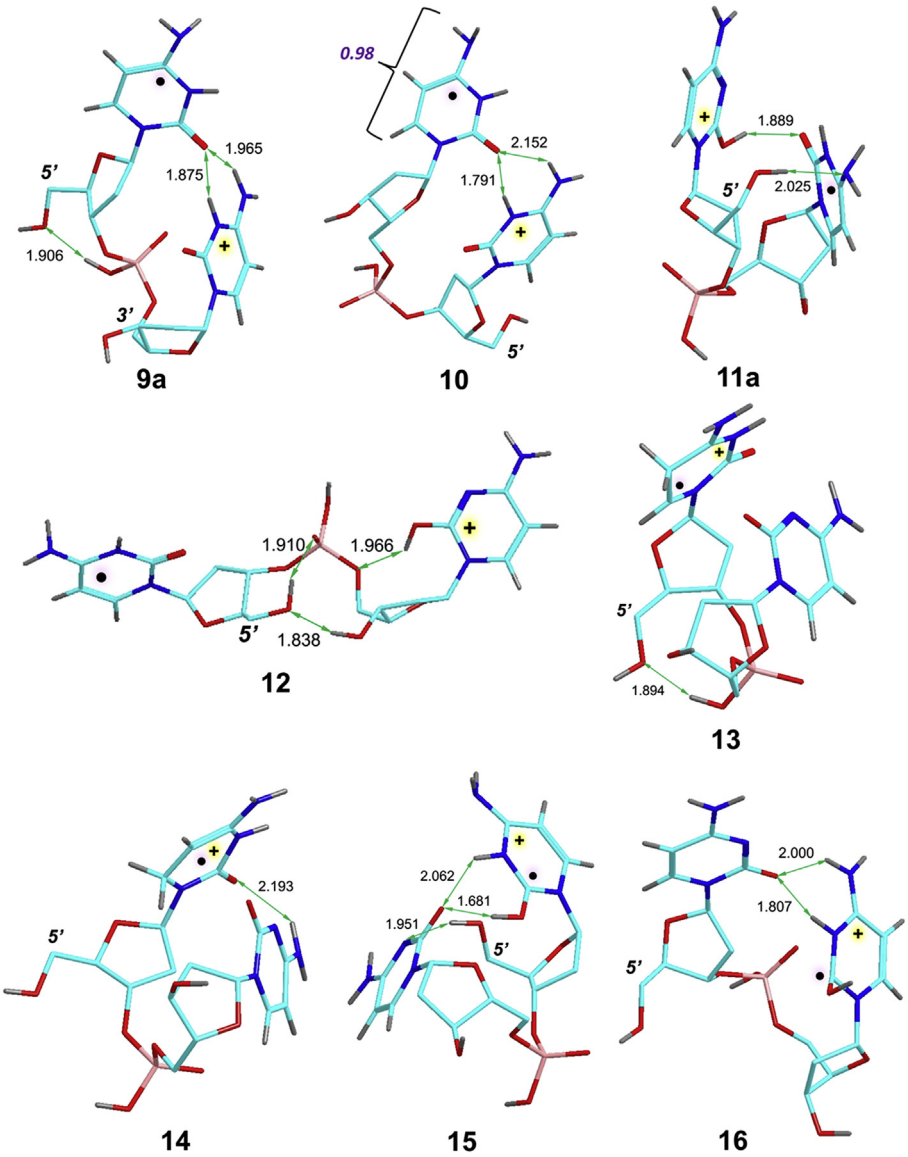

Fig. 5. M06-2X/6-31 + G (d,p) optimized structures of low-energy $(dCC + 2H)^{+\bullet}$. Color coding is as in Fig. 4. Major hydrogen bonds are indicated by green arrows with distances in Ångstrøms. The sum of atomic spin densities is shown for structure **10**. (For interpretation of the references to color in this figure legend, the reader is referred to the Web version of this article.)

consistent with the previously reported conformational collapse in other dinucleotide cation radicals [12,13].

In addition to the canonical cation radicals that can be directly produced by electron attachment to the dications, we also investigated structures resulting from proton or hydrogen atom transfer between the cytosine units. Hydrogen atom migration to C-5 of the 5′-cytosine formed cation radical **13** (Fig. 5) that was 34 kJ mol^{-1} less stable than **9a**. An analogous H-atom migration to the C-6 position formed an even less stable radical **14** at 58 kJ mol^{-1} relative to **9a**. Proton migration to the 5′- and 3′-radical cytosine ring produced dihydrocytosine cation radicals **15** and **16**, respectively (Fig. 5). However, these were substantially less stable than **9a** (Table 2).

The reaction energies of $(dCC + 2H)^{+\bullet}$ were calculated for the main channels and referenced to the lowest energy structure **9a**. Isomerization by a migration of the 3′-N-3-H cytosine proton to C-5 in the 5′-cytosine (**13**, Scheme 2) was calculated to have a low TS energy (103 kJ mol^{-1}) and can proceed in **9a** at the initial mean vibrational energy of 280 k mol^{-1} provided by ETD (vide supra). RRKM calculations of the rate constant for the isomerization in **9a** (Figure S3a) indicated a relatively slow reaction that would achieve ca. 20% conversion at 280 kJ mol^{-1}. However, the reverse isomerization of **13** to **9a** was 34 kJ mol^{-1} exothermic and fast, favoring **9a** by a factor of >100 over a broad range of internal energies (Figure S3b). Loss of water was the lowest-energy dissociation of $(dCC + 2H)^{+\bullet}$, requiring a threshold energy of 130 kJ mol^{-1} from **9a** to form ion **17** (Scheme 2). An isomer of $(dCC - H_2O + 2H)^{+\bullet}$ in which the 3′-cytosine was cyclized to the 5′-position (**18**) was also considered, but it was calculated to be 58 kJ mol^{-1} less stable than ion **17**. The low threshold energy for the formation of **17** was consistent with the dominant loss of water from $(dCC + 2H)^{+\bullet}$ upon CID (Fig. 1b). Considering the estimated initial excitation of the ETD-formed $(dCC + 2H)^{+\bullet}$ (280 kJ mol^{-1}, vide supra), it was not surprising that upon ETD of the complex, a fraction of the cation radicals underwent water elimination (cf. Fig. 1a) in competition with collisional cooling. A further dissociation of ion **17** forming the w_1 ion (**19**, *m/z* 308) and a_1 radical (**20**) was a low-energy process for which we calculated a threshold energy of 154 kJ mol^{-1}. This backbone cleavage competed with the loss of the 3′-guanine base (*m/z* 389, Fig. 1c) with a threshold energy of 130 kJ mol^{-1} (Table 2). We note that the energetics of these competing dissociations was more realistically captured by MP2 calculations (Table 2).

3.5. Calculated absorption spectra and action spectra assignment

We used the optimized structures of $(dCC + 2H)^{+\bullet}$ ions for TD-DFT calculations of excitation energies and oscillator strength. M06-2X and ωB97X-D TD-DFT calculations gave very similar results for the excited states, and so only the former are presented here. Likewise, applying the larger 6-311++G (2d,p) basis set in the TD-DFT M06-2X calculations gave data that were very similar to those from calculations with the 6-31 + G (d,p) basis set, as illustrated with **15** (Figure S4). The absorption spectra of the lowest-energy 5′-N-3-H-cytosine radicals (**9a** and **9b**) showed weak bands in the 550-600 and 390-410 nm regions. Several weak bands were also found in 270-330 nm region (Fig. 6). The main absorption lines appeared in the 230-260 nm region of the spectrum. The line wavelengths and oscillator strength differed for **9a** and **9b**, indicating that the spectra were sensitive to the cation radical conformation. However, band broadening by vibronic transitions was likely to obscure the differences, as indicated by the simulated absorption peaks that were artificially broadened by convolution of

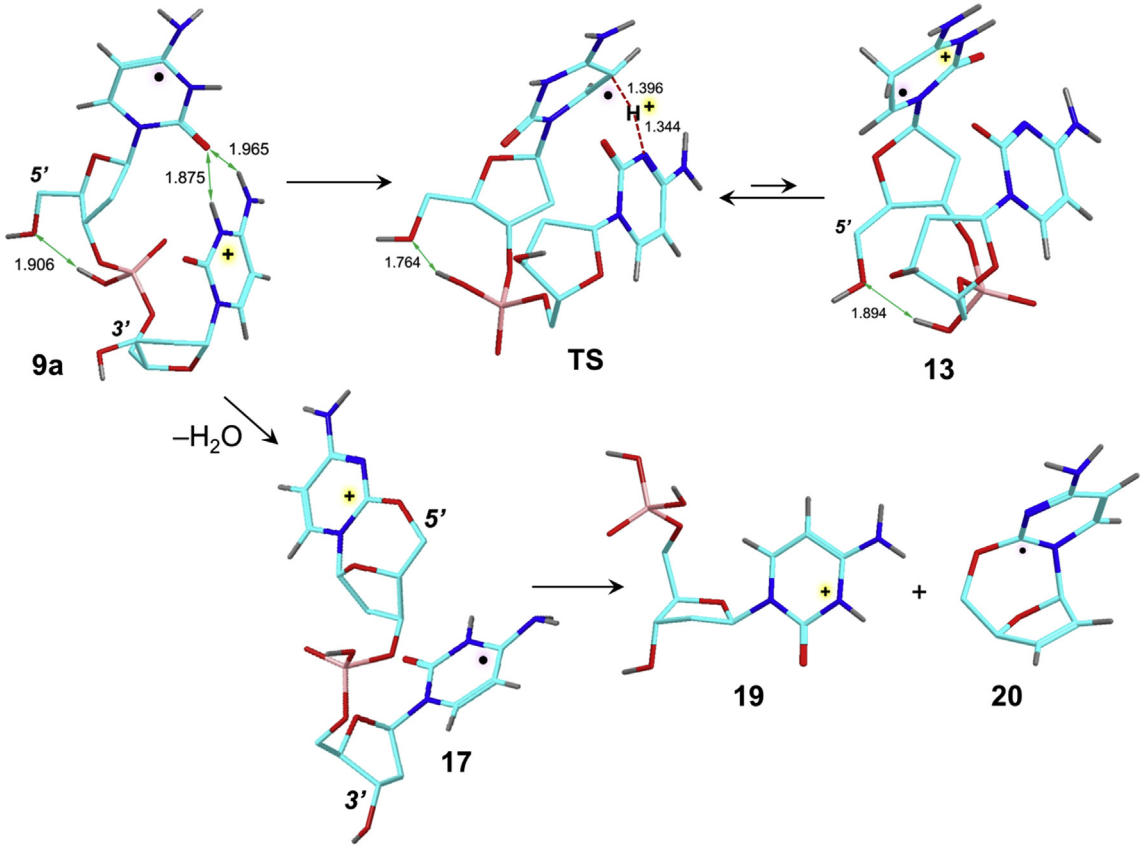

Scheme 2. Isomerization and dissociation of $(dCC + 2H)^{+\bullet}$ cation radical **9a**.

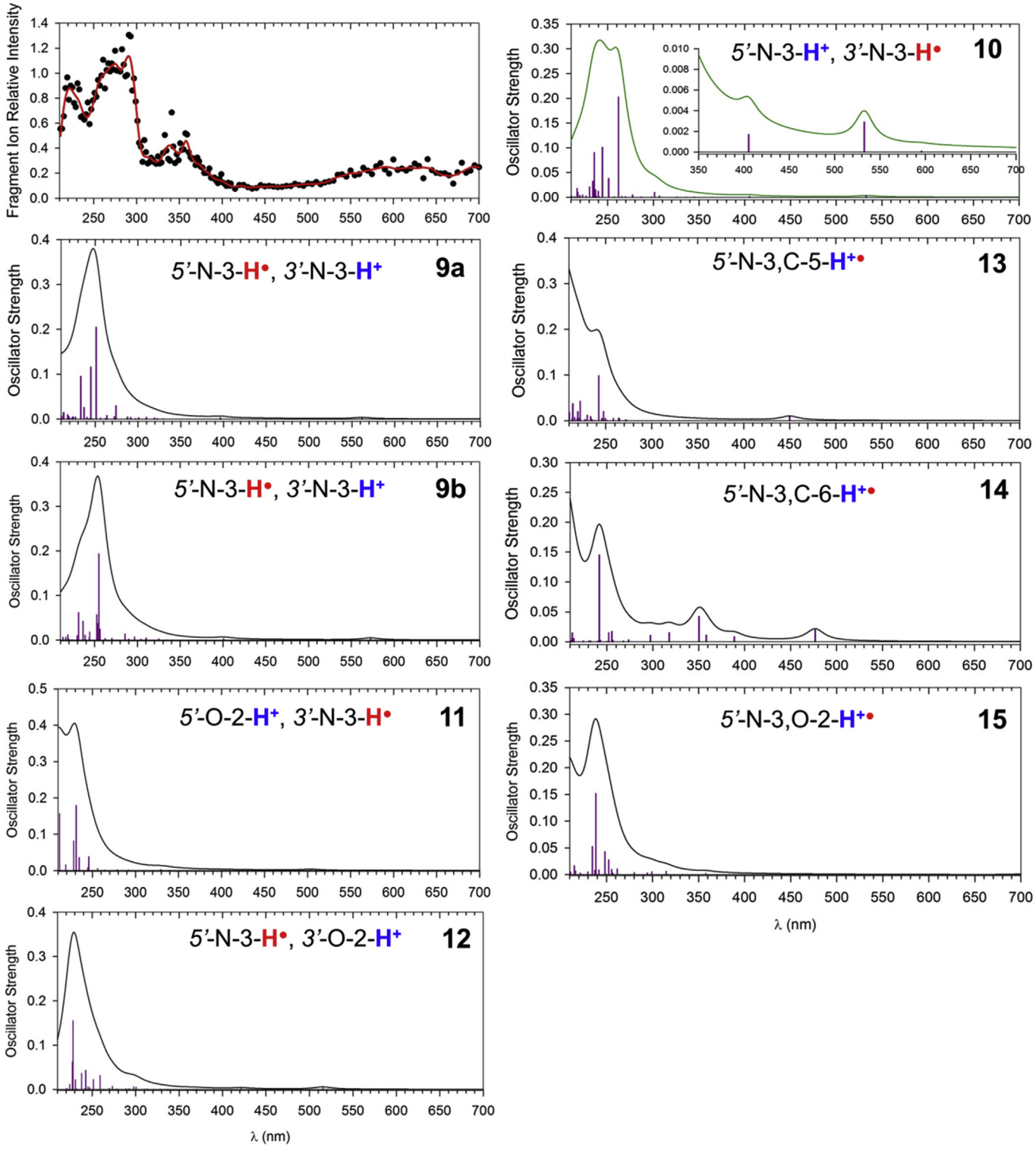

Fig. 6. Action and TD-DFT absorption spectra of $(dCC + 2H)^{+\bullet}$ ions. The nucleobase 5′ or 3′ positions are denoted by italics.

Lorentzian functions at 12 nm full width at half maximum (Fig. 6). The spectrum of the isomeric 3′-N-3-H-cytosine radical (**10**) displayed the main line at 260 nm which resulted in a different band pattern even after broadening. The absorption spectra of the 3′-N-3-H$^{\bullet}$ radicals having the 5′-ring protonated at O-2 (**11a**, **11b**) showed distinct features in the 210-300 nm region. In particular, the spectra displayed a blue shift of the main lines and different pattern of the weak lines at 250-330 nm. A blue shift in the 210-250 nm region was also observed for the 5′-N-3-H$^{\bullet}$ radical having the 3′-ring protonated at O-2 (**12**). The spectrum of the 5,5-H_2 isomer **13** had an absorption band at 450 nm and stronger bands at $\lambda < 250$ nm (Fig. 6). The 6,6-H_2 isomer (**14**) gave a still different spectrum, showing prominent bands at 476 and 350 nm and other bands in the 300-400 nm region. Finally, the 5′-N-3, O-2-H cation

radical (**15**) showed no bands above 360 nm, with main absorption appearing in the 230-250 nm region and at wavelengths < 200 nm (Fig. 6).

A comparison of the action spectrum with the calculated absorption spectra revealed both matches and discrepancies. The 220-nm band had counterparts in the absorption spectra of **11** and **13**. Although we did not calculate multiple vibronic spectra for the isomers, we note that vibronic transitions typically result in a red shift and band broadening. Thus electron transitions in several isomers with $\lambda < 200$ nm may appear at 220 nm in the action spectrum. The 270 and 290 nm bands in the action spectrum are usually not much diagnostic for DNA oligonucleotide cation radicals [12,13]. Considering the vibronic red shift, the absorption spectrum of **10** showed the closest match of the dual-peak band at 240 and 260 nm with the corresponding bands in the action spectrum. The 350-nm band in the action spectrum was the most difficult one to match. Although most of the low-energy $(dCC + 2H)^{+\bullet}$ isomers showed multiple transitions in this region of the spectrum, the bands had low oscillation strength to match the experimental band. The C-6-H radical **14** was the only isomer displaying a strong band at 350 nm in the absorption spectrum; however, **14** was a high-energy isomer (Table 2) that would be difficult to form by a rearrangement of an ETD-produced cation-radical. The broad bands at $\lambda > 550$ nm in the action spectrum had analogical absorption bands in the spectra of **9a**, **9b**, **10**, **11**, and **12,** although those were less intense. We observed previously that the calculated intensities of long-wavelength bands of DNA radicals were very sensitive to the vibrational states and often displayed a substantial increase due to vibronic transitions [61]. In summary, none of the calculated TD-DFT absorption spectra showed a match with the action spectrum that would be comparable to results obtained for other DNA radicals [13,14].

The radical energetics and correlation with precursors and intermediates suggested ions **9a**, **9b** as the most likely species produced by ETD. A notable feature of their chemistry was the facile loss of water forming the *m/z* 500 ion (Fig. 1a and b). We used this fragment ion and its possible structure relationship with **9a**, **9b** to characterize the $(dCC + 2H)^{+\bullet}$ ions. The UV-Vis action spectrum of the $(dCC - H_2O + 2H)^{+\bullet}$ ion displayed bands at 220, 270, 330, 430, and 530 nm (Fig. 3a) that were composed of the photofragment ion intensities at *m/z* 308 and 292 (Fig. 1c). The action spectrum showed a close match with the TD-DFT absorption spectrum of a cation radical produced by loss of the 5′-OH group with cyclization onto the 5′-cytosine ring, forming a cyclocytidine structure (**17**, Scheme 2, Fig. 3b). In contrast, the absorption spectrum of the 3′→5′ cyclized isomer (**18**) was distinctly different and did not exhibit matching features with the action spectrum of the $(dCC - H_2O + 2H)^{+\bullet}$ ion. The reactant (**9a**) and product (**17**) displayed different electron distributions in the 3′- and 5′-cytosine rings. Although we did not study the details of the ring formation and the pertinent transition state, the development of the electron density in **17** reflected the ground electronic state that favored the charged 5′-cyclocytosine and a radical 3′-cytosine ring. The close match of the absorption spectrum of **17** and its reaction correspondence with structure **9a** and its conformers provided corroborative evidence for the $(dCC + 2H)^{+\bullet}$ ions having a 5′-N-3-H$^{\bullet}$, 3′-N-3-H^{+} arrangement of the charged and radical cytosine rings.

4. Conclusions

The experimental and computational data reported here allowed us to arrive at the following conclusions. Stable hydrogen-rich deoxycytidine dinucleotide cation radicals can be generated in the gas phase by electron transfer dissociation of doubly charged dCC-crown-ether complexes. Upon activation, the cation radicals undergo dissociations involving radical losses. Photodissociation in the 210-700 nm wavelength range yielded action spectra that were interpreted after extensive modeling of precursor dication and cation-radical structures. Although the experimental and calculated spectra did not achieve a flawless match, corroborating evidence from fragment ion action spectra and energy analysis led us to conclude that the $(dCC + 2H)^{+\bullet}$ ions had the N-3-H tautomeric pattern in both the protonated and H-atom adducted cytosine rings. The 5′-N-3-H$^{\bullet}$, 3′-N-3-H^{+} distribution of the cytosine radical and charge sites was preferred energetically, but could not be resolved by UV-vis action spectroscopy alone because of the similarity of the electronic transitions in isomers differing in the radical and charge position.

Acknowledgments

Financial support was provided by the Chemistry Division of the National Science Foundation, Grants CHE-1661815 for experiments and CHE-1624430 for computations. F.T. acknowledges the Klaus and Mary Ann Saegebarth Endowment for general support.

Appendix A. Supplementary data

Supplementary data to this article can be found online at https://doi.org/10.1016/j.ijms.2019.05.016.

References

[1] B. Boudaiffa, P. Cloutier, D. Hunting, M.A. Huels, L. Sanche, Resonant formation of DNA strand breaks by low-energy (3 to 20 eV) electrons, Science 287 (5458) (2000) 1658–1662.
[2] K. Aflatooni, G.A. Gallup, P.D. Burrow, Electron attachment energies of the DNA bases, J. Phys. Chem. A 102 (1998) 6205–6207.
[3] A.F. Jalbout, L. Adamowicz, Electron attachment to DNA base complexes, Adv. Quant. Chem. 52 (2007) 231–252.
[4] L.S. Myers Jr., M.L. Hollis, L.M. Theard, Pulse radiolysis of DNA and related pyrimidine compounds: reactions of the OH radical, Adv. Chem. 81 (1968) 345–367.
[5] G. Nucifora, B. Smaller, R. Remko, E.C. Avery, Transient radicals of DNA bases by pulse radiolysis. Effects of cysteine and cysteamine as radioprotectors, Radiat. Res. 49 (1972) 96–111.
[6] K. Hildebrand, D. Schulte-Frohlinde, ESR spectra of radicals of single-stranded and double-stranded DNA in aqueous solution. Implications for hydroxyl radical-induced strand breakage, Free Radic. Res. Commun. 11 (1990) 195–206.
[7] J.K. Wolken, E.A. Syrstad, S. Vivekananda, F. Tureček, Uracil radicals in the gas phase. Specific generation and energetics, J. Am. Chem. Soc. 123 (2001) 5804–5805.
[8] E.A. Syrstad, S. Vivekananda, F. Tureček, Direct observation of a hydrogen atom adduct to C-5 in uracil. A neutralization-reionization mass spectrometric and ab initio study, J. Phys. Chem. A 105 (2001) 8339–8351.
[9] J.K. Wolken, F. Tureček, Direct observation of a hydrogen atom adduct to O-4 in uracil. A neutralization-reionization mass spectrometric and ab initio study, J. Phys. Chem. A 105 (2001) 8352–8360.
[10] X. Chen, E.A. Syrstad, M.T. Nguyen, P. Gerbaux, F. Tureček, Adenine radicals in the gas phase. An experimental and computational study of hydrogen atom adducts to adenine, J. Phys. Chem. A 109 (2005) 8121–8132.
[11] F. Tureček, Computational studies of radicals relevant to nucleic acid damage, Adv. Quant. Chem. 52 (2007) 89–120.
[12] J.A. Korn, J. Urban, A. Dang, H.T.H. Nguyen, F. Turecek, UV-vis action spectroscopy reveals a conformational collapse in hydrogen-rich dinucleotide cation radicals, J. Phys. Chem. Lett. 8 (2017) 4100–4107.
[13] Y. Liu, J.A. Korn, A. Dang, F. Turecek, Hydrogen-rich cation radicals of DNA dinucleotides. Generation and structure elucidation by UV-vis action spectroscopy, J. Phys. Chem. B 122 (2018) 9665–9680.
[14] C.J. Shaffer, R. Pepin, F. Tureček, Combining UV photodissociation action spectroscopy with electron transfer dissociation for structure analysis of gas-phase peptide cation-radicals, J. Mass Spectrom. 50 (2015) 1438–1442.
[15] N.C. Polfer, P. Dugourd (Eds.), Laser Photodissociation and Spectroscopy of Mass Separated Biomolecular Ions; Lecture Notes in Chemistry vol.83, Springer, Cham, 2013, pp. 13–20.
[16] R. Antoine, P. Dugourd, UV-visible activation of biomolecular ions. (Laser photodissociation and spectroscopy of mass-separated biomolecular ions), Lect. Notes Chem. 83 (2013) 93–116.
[17] O. Kostko, K. Bravaya, A. Krylov, M. Ahmed, Ionization of cytosine monomer and dimer studied by VUV photoionization and electronic structure

calculations, Phys. Chem. Chem. Phys. 12 (2010) 2860–2872.
[18] Z. Chen, K.-C. Lau, G.A. Garcia, L. Nahon, D.K. Bozanic, L. Poisson, M.M. Al-Mogren, M. Schwell, J.S. Francisco, A. Bellili, M. Hochlaf, Identifying cytosine-specific isomers via high-accuracy single photon ionization, J. Am. Chem. Soc. 138 (2016) 16596–16599.
[19] J.L. Alonso, V. Vaquero, I. Pena, J.C. Lopez, S. Mata, W. Caminati, All five forms of cytosine revealed in the gas phase, Angew. Chem. Int. Ed. 52 (2013) 2331–2334.
[20] M.J. Scanlan, I.H. Hillier, Accurate prediction of the relative energies of the tautomers of cytosine in the gas phase and in aqueous solution, J. Chem. Soc., Chem. Commun. (1984) 102–103.
[21] J.S. Kwiatkowski, R.J. Bartlett, W.B. Person, Contributions from electron correlation to the relative stabilities of the tautomers of nucleic acid bases, J. Am. Chem. Soc. 110 (1988) 2353–2358.
[22] I.R. Gould, D.V.S. Green, P. Young, I.H. Hillier, A theoretical study using ab initio methods of tautomerism in cytosine in the gas phase and in water, J. Org. Chem. 57 (1992) 4434–4437.
[23] R. Kobayashi, A CCSD(T) study of the relative stabilities of cytosine tautomers, J. Phys. Chem. A 102 (1998) 10813–10817.
[24] S.A. Trygubenko, T.V. Bogdan, M. Rueda, M. Orozco, F.J. Luque, J. Sponer, P. Slavicek, P. Hobza, Correlated ab initio study of nucleic acid bases and their tautomers in the gas phase, in a microhydrated environment and in aqueous solution. Part 1. Cytosine, Phys. Chem. Chem. Phys. 4 (2002) 4192–4203.
[25] M. Lesslie, J.T. Lawler, A. Dang, J.A. Korn, D. Bím, V. Steinmetz, P. Maitre, F. Tureček V. Ryzhov, Cytosine radical cation: a gas-phase study combining IRMPD spectroscopy, UV-PD spectroscopy, ion-molecule reactions, and theoretical calculations, ChemPhysChem 18 (2017) 1293–1301.
[26] J.K. Wolken, C. Yao, F. Turecek, M.J. Polce, C. Wesdemiotis, Cytosine neutral molecules and cation-radicals in the gas-phase. structures, energetics, ion chemistry, and neutralization-reionization mass spectrometry, Int. J. Mass Spectrom. 267 (2007) 30–42.
[27] A. Filippie, C. Fraschetti, F. Rondino, S. Piccirillo, V. Steinmetz, L. Guidoni, M. Speranza, Protonated pyrimidine nucleosides probed by IRMPD spectroscopy, Int. J. Mass Spectrom. 354 (2013) 54–61.
[28] J.Y. Salpin, S. Guillaumont, J. Tortajada, L. MacAleese, J. Lemaire, P. Maitre, Infrared spectra of protonated uracil, thymine and cytosine, ChemPhysChem 8 (2007) 2235–2244.
[29] J.M. Bakker, J.-Y. Salpin, P. Maitre, Tautomerism of cytosine probed by gas phase IR spectroscopy, Int. J. Mass Spectrom. 283 (2009) 214–221.
[30] M. Broquier, S. Soorkia, G. Pino, C. Dedonder-Lardeux, C. Jouvet, G. Gregoire, Excited state dynamics of cold protonated cytosine tautomers characterization of charge transfer, intersystem crossing, and internal conversion processes, J. Phys. Chem. A 121 (2017) 6429–6439.
[31] R.R. Wu, B. Yang, C.E. Frieler, G. Berden, J. Oomens, M.T. Rodgers, N3 and O2 protonated tautomeric conformations of 2'-deoxycytidine and cytidine coexist in the gas phase, J. Phys. Chem. B 119 (2015) 5773–5784.
[32] R.R. Wu, L.A. Hamlow, C.C. He, Y.-W. Nei, G. Berden, J. Oomens, M.T. Rodgers, N3 and O2 protonated conformers of the cytosine mononucleotides coexist in the gas phase, J. Am. Soc. Mass Spectrom. 28 (2017) 1638–1646.
[33] C. Yao, F. Tureček, M.J. Polce, C. Wesdemiotis, Proton and hydrogen atom adducts to cytosine. An experimental and computational study, Int. J. Mass Spectrom. 265 (2007) 106–123.
[34] C. Yao, M. Cuadrado-Peinado, M. Polášek, F. Tureček, Specific generation of 1-methylcytosine radicals in the gas-phase, Angew Chem. Int. Ed. Engl. 44 (2005) 6708–6711.
[35] F. Tureček, C. Yao, Hydrogen atom addition to cytosine, 1-methylcytosine, and cytosine-water complexes. A computational study of a mechanistic dichotomy, J. Phys. Chem. A 107 (2003) 9221–9231.
[36] J.D. Zhang, Y. Xie, H.F. Schaefer III, Q. Luo, Q.-S. Li, Addition of hydrogen atom/hydride anion to the double bonds of cytosine tautomers: radical and anion structures and energetics, Mol. Phys. 104 (2006) 2347–2366.
[37] K. Tomic, J. Tatchen, C.M. Marian, Quantum chemical investigation of the electronic spectra of the keto, enol, and keto-imine tautomers of cytosine, J. Phys. Chem. A 109 (2005) 8410–8418.
[38] G. Bazso, G. Tarczay, G. Fogarasi, P.G. Szalay, Tautomers of cytosine and their excited electronic states: a matrix isolation spectroscopic and quantum chemical study, Phys. Chem. Chem. Phys. 13 (2011) 6799–6807.
[39] K. Kosma, C. Schroeter, E. Samoylova, I.V. Hertel, T. Schultz, Excited-state dynamics of cytosine tautomers, J. Am. Chem. Soc. 131 (2009) 16939–16943.
[40] W. Ho Jr., H.-C. Yen, W.-K. Chou, C.-N. Weng, L.-H. Cheng, H.-Q. Shi, S.-H. Lai, P.-Y. Cheng, Disentangling intrinsic ultrafast excited-state dynamics of cytosine tautomers, J. Phys. Chem. A 115 (2011) 8406–8418.
[41] A. Domingo, A. Rodriguez-Fortea, C. de Graaf, The absorption spectrum of cytosine tautomers: beyond the static approach, J. Chem. Theory Comput. 8 (2012) 235–244.
[42] S. Lobsiger, M.A. Trachsel, H.-M. Frey, S. Leutwyler, Excited-state structure and dynamics of keto-amino cytosine: the $1\pi\pi^*$ state is nonplanar and its radiationless decay is not ultrafast, J. Phys. Chem. B 117 (2013) 6106–6115.
[43] A. Nakayama, Y. Harabuchi, S. Yamazaki, T. Taketsugu, Photophysics of cytosine tautomers: new insights into the nonradiative decay mechanisms from MS-CASPT2 potential energy calculations and excited-state molecular dynamics simulations, Phys. Chem. Chem. Phys. 15 (2013) 12322–12339.
[44] C.G. Triandafillou, S. Matsika, Excited-state tautomerization of gas-phase cytosine, J. Phys. Chem. A 117 (2013) 12165–12174.
[45] J. Martens, G. Berden, C.R. Gebhardt, J. Oomens, Infrared ion spectroscopy in a modified quadrupole ion trap mass spectrometer at the FELIX free electron laser laboratory, Rev. Sci. Instrum. 87 (2016) doi: 103108/1-103108.
[46] A. Dang, J.A. Korn, J. Gladden, B. Mozzone, F. Turecek, J. Am. Soc. Mass Spectrom. 30 (2019), https://doi.org/10.1007/s13361-019-02229-z in press.
[47] J.J.P. Stewart, Optimization of parameters for semi-empirical methods V: modification of NDDO approximations and applications to 70 elements, J. Mol. Model. 13 (2007) 1173–1213.
[48] J. Řezáč, J. Fanfrlík, D. Salahub, P. Hobza, Semi-empirical quantum chemical PM6 method augmented by dispersion and H bonding correction terms reliably describes various types of noncovalent complexes, J. Chem. Theory Comput. 5 (2009) 1749–1760.
[49] H.J. Berendsen, J.V. Postma, W.F. van Gunsteren, A.R.H.J. DiNola, J.R. Haak, Molecular dynamics with coupling to an external bath, J. Chem. Phys. 81 (1984) 3684–3690.
[50] J.J.P. Stewart, MOPAC 16, Stewart Computational Chemistry, Colorado Springs: CO, 2016.
[51] J. Řezáč, Cuby: an integrative framework for computational chemistry, J. Comput. Chem. 37 (2016) 1230–1237.
[52] A.D. Becke, Density-functional exchange-energy approximation with correct asymptotic behavior, Phys. Rev. 38 (1988) 3098–3100.
[53] J.D. Chai, M. Head-Gordon, Long-range corrected hybrid density functionals with damped atom-atom dispersion corrections, Phys. Chem. Chem. Phys. 10 (2008) 6615–6620.
[54] Y. Zhao, D.G. Truhlar, The M06 suite of density functionals for main group thermochemistry, thermochemical kinetics, noncovalent interactions, excited states, and transition elements: two new functionals and systematic testing of four M06-class functionals and 12 other functionals, Theor. Chem. Accounts 120 (2008) 215–241.
[55] C. Møller, M.S. Plesset, A note on an approximation treatment for many-electron systems, Phys. Rev. 46 (1934) 618–622.
[56] H.B. Schlegel, Potential energy curves using unrestricted Moller-Plesset perturbation theory with spin annihilation, J. Chem. Phys. 84 (1986) 4530.
[57] I. Mayer, Spin-projected UHF method. IV. Comparison of potential curves given by different one-electron methods, Adv. Quant. Chem. 14 (1978) 29–38.
[58] P.J. Knowles, J.S. Andrews, R.D. Amos, N.C. Handy, J.A. Pople, Restricted Moller-Plesset theory for open shell molecules, Chem. Phys. Lett. 186 (1991) 130–136.
[59] J. Tomasi, B. Mennucci, R. Cammi, Quantum mechanical continuum solvation models, Chem. Rev. 105 (2005) 2999–3093.
[60] F. Furche, A. Ahlrichs, Adiabatic time-dependent density functional methods for excited state properties, J. Chem. Phys. 117 (2002) 7433–7447.
[61] A. Dang, Y. Liu, F. Tureček, UV-vis action spectroscopy of guanine, 9-methylguanine and 2'-deoxyguanosine cation radicals in the gas phase, J. Phys. Chem. A 123 (2019) 3272–3284.
[62] M.J. Frisch, G.W. Trucks, H.B. Schlegel, G.E. Scuseria, M.A. Robb, J.R. Cheeseman, G. Scalmani, V. Barone, G.A. Petersson, H. Nakatsuji, M. Caricato, A.V. Marenich, J. Bloino, B.G. Janesko, R. Gomperts, B. Mennucci, H.P. Hratchian, J.V. Ortiz, A.F. Izmaylov, J.L. Sonnenberg, D. Williams-Young, F. Ding, F. Lipparini, F. Egidi, J. Goings, B. Peng, A. Petrone, T. Henderson, D. Ranasinghe, V.G. Zakrzewski, J. Gao, N. Rega, G. Zheng, W. Liang, H. Hada, M. Ehara, K. Toyota, R. Fukuda, J. Hasegawa, M. Ishida, T. Nakajima, Y. Honda, O. Kitao, H. Nakai, T. Vreven, K. Throssell, J.A. Montgomery Jr., J.E. Peralta, F. Ogliaro, M.J. Bearpark, J.J. Heyd, E.N. Brothers, K.N. Kudin, V.N. Staroverov, T.A. Keith, R. Kobayashi, J. Normand, K. Raghavachari, A.P. Rendell, J.C. Burant, S.S. Iyengar, J. Tomasi, M. Cossi, J.M. Millam, M. Klene, C. Adamo, R. Cammi, J.W. Ochterski, R.L. Martin, K. Morokuma, O. Farkas, J.B. Foresman, D.J. Fox, Gaussian 16, Revision A01, Gaussian, Inc., Wallingford CT, 2016.
[63] J.E.P. Syka, J.J. Coon, M.J. Schroeder, J. Shabanowitz, D.F. Hunt, Peptide and protein sequence analysis by electron transfer dissociation mass spectrometry, Proc. Natl. Acad. Sci. U. S. A 101 (2004) 9528–9533.
[64] K.K. Murray, DNA sequencing by mass spectrometry, J. Mass Spectrom. 31 (1996) 1203–1215.
[65] S.A. McLuckey, G.J. Van Berkel, G.L. Glish, Tandem mass spectrometry of small, multiply charged oligonucleotides, J. Am. Soc. Mass Spectrom. 3 (1992) 60–70.
[66] A.I.S. Holm, M.K. Larsen, S. Panja, P. Hvelplund, S.B. Nielsen, R.D. Leib, W.A. Donald, E.R. Williams, C. Hao, F. Tureček, Electron capture, femtosecond electron transfer and theory: a study of noncovalent crown ether 1,n-diammonium alkane complexes, Int. J. Mass Spectrom. 276 (2008) 116–126.
[67] J. Michl, Electronic structure of non-alternant hydrocarbons: their analogues and derivatives, J. Mol. Spectrosc. 30 (1969) 68–76.
[68] F. Tureček, R.R. Julian, Peptide radicals and cation-radicals in the gas phase, Chem. Rev. 113 (2013) 6691–6733.
[69] R. Pepin, F. Turecek, Kinetic ion thermometers for electron transfer dissociation, J. Phys. Chem. B 119 (2015) 2818–2826.
[70] D.E. Goeringer, S.A. McLuckey, Relaxation of internally excited high-mass ions simulated under typical quadrupole ion trap storage conditions, Int. J. Mass Spectrom. 177 (1998) 163–174.